Mechatronic Design and Characterization of the Index Finger Module of a Hand Exoskeleton for Post-Stroke Rehabilitation

Azzurra Chiri, Nicola Vitiello, *Student Member, IEEE*, Francesco Giovacchini, Stefano Roccella, Fabrizio Vecchi, *Member, IEEE*, and Maria Chiara Carrozza, *Associate Member, IEEE*

***Abstract*—This paper presents HANDEXOS, a novel wearable multiphalanges device for post-stroke rehabilitation. It was designed in order to allow for a functional and safe interaction with the user's hand by means of an anthropomorphic kinematics and the minimization of the human/exoskeleton rotational axes misalignment. This paper describes the mechatronic design of the exoskeleton's index finger module, simulation, modeling, and development of the actuation unit and sensory system. Experimental results on the validation of the dynamic model and experimental characterization of the index finger module with healthy subjects are reported, showing promising results that encourage further clinical trials.**

***Index Terms*—Axes misalignment, Bowden cables, hand exoskeleton, hand rehabilitation, underactuation.**

I. Introduction

STROKE is the major cause of adult long-term disability in Europe and many other countries, so medical and social care consume a huge amount of healthcare resources [1] both for the direct costs related to hospital and home assistance, and for the indirect costs due to inactivity of the affected subjects [2]. Robot-mediated rehabilitation supports the physicians in providing high-intensity and repetitive therapy. In this way, the patient can receive benefits from the rehabilitation process, while therapists can reduce their workload. Moreover, robotic devices offer an objective, reliable tool to monitor patient's progress and to accurately assess their motor function [3]. Based on this idea, robot-aided neurorehabilitation was widely investigated and proved to be good as or even better than conventional therapy [4].

In particular, one of the main needs of chronic stroke patients is the hand motor function restoration. Indeed, in the last years, different robotic systems for hand assistance and rehabilitation have been developed. Some of these devices have been tested with stroke users, showing improvements that justify further investigation in the use of rehabilitation robotics for hand motor therapy [5]–[7]. Although robotic treatment positively influences hand recovery, there is not a single treatment strategy or protocol, so different robots have been designed to administer alternative therapies.

One category is represented by devices that train opening and closing movements of the entire hand: the HWARD [5], a 3-degrees of freedom (DOFs) pneumatically actuated device, has been proved to enhance grasping and releasing hand abilities and to increase sensorimotor cortex activation across the period of therapy. The haptic knob [6] uses an actuated parallelogram structure that presents two movable surfaces that are squeezed by the subject. The Hand Robot Alpha-Prototype II [7] uses a double crank and slider mechanism encased in a variable-radius cylindrical cover. The disadvantage of this category is the limited control of the fingers joints, which may lead to physiologically inaccurate joint kinematics.

An alternate approach bases on pneumatically actuated hand gloves with the unidirectional mode of actuation (finger extension) that apply torques to the finger joints through electropneumatic servo valve. This is, for example, the case of the Rutgers Master II [8] that uses custom pneumatic actuators arranged in a direct-drive configuration in the palm and can simulate a virtual object if the subject is able to close the hand. Another pneumatic glove is described in [9], which is made of an air bladder and channels that run along the palmar side of the hand to provide assistance in finger extension. The disadvantage of such approach is the fixed and not adjustable ratio of torques applied to the finger joints.

Another approach that overpasses the limitations of the aforementioned categories consists of powered gloves and exoskeletal machines [10]–[21]. These devices, despite their high complexity, can assist each finger independently and control position and torque of each joint. State-of-the-art hand exoskeletons can be classified into two functional categories depending on the possibility to interact with each user's finger in one or multiple contact points. With the first approach forces are applied to the distal segments of each finger (e.g., the fingertip) [10]–[13], so the exoskeleton is conceived as a serial robotic manipulator that works in parallel to each human finger. The main advantage of such approach is that any issue related to joint axes alignment between human hand and robot is solved by leaving free any

Manuscript received September 12, 2010; revised December 22, 2010 and March 15, 2011; accepted April 2, 2011. Recommended by Technical Editor E. Richer. This work was supported in part by the EU within the NEUROBOTICS Integrated Project (The fusion of NEUROscience and roBOTICS, IST-FET under Project #2003-001917) and the EVRYON Collaborative under Project STREP (FP7-ICT-2007-3-231451).

The authors are with The BioRobotics Institute, Scuola Superiore di Studi Universitari e di Perfezionamento Sant'Anna, 56127 Pisa, Italy (e-mail a.chiri@sssup.it; n.vitiello@sssup.it; f.giovacchini@arts.sssup.it; s.roccella@sssup.it; fabrizio.vecchi@arts.sssup.it; carrozza@sssup.it).

Color versions of one or more of the figures in this paper are available online at http://ieeexplore.ieee.org.

Digital Object Identifier 10.1109/TMECH.2011.2144614

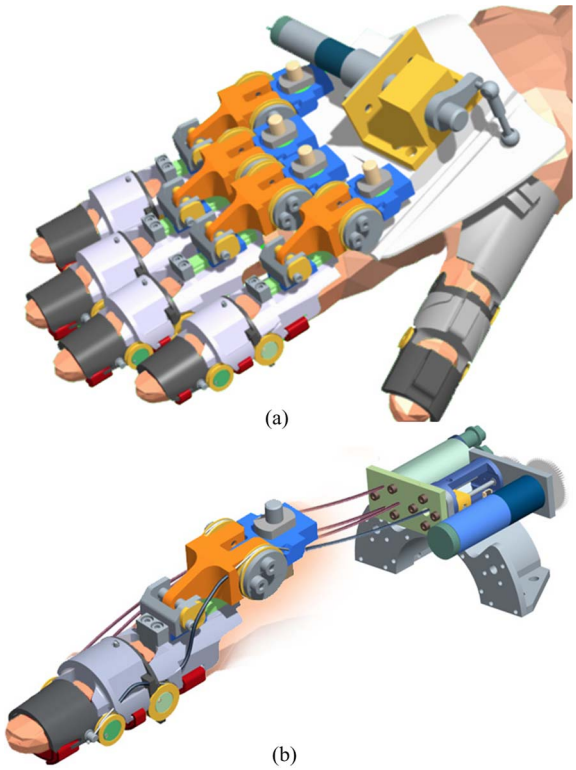

Fig. 1. (a) Concept of HANDEXOS: five independent finger modules including the thumb. (b) Detail of the index finger module with relative actuation unit.

possible relative motion. On the other hand, this solution does not allow for an accurate control of the position and torque on each finger joint.

The second approach, instead, consists of a multiple-point interaction between the device and the user's hand [14]–[21]. This is the aim we pursued with HANDEXOS (see Fig. 1), whose concept was preliminary described in [22].

The critical design issue of the multiple-point approach is the kinematic coupling between the robotic device and the user's hand. In fact, in this case, each finger is linked to the device in more than one point, so that relative motion for the alignment of the correspondent finger and exoskeleton rotational axes is not allowed. As a consequence, any joint-axes misalignment can cause undesired translational forces on human articulations [23] that, if not controlled, can lead to an uncomfortable or even painful use of the device.

In the design of HANDEXOS, we considered the joint axes misalignment issue with a main focus on the metacarpo–phalangeal (MCP) joint whose complex anatomy makes difficult to assure good axes alignment during the extension/flexion task. In particular, we conceived a slider-crank-like mechanism that transmits the driving torque onto the human MCP joint, while minimizing the undesired forces loading such articulation.

Another common limitation of hand rehabilitation devices, conceived according to either the single or multiple-point interaction design approaches, is the high overall size and inertia of the moving parts, which is partly responsible for a low functionality and user acceptability [10]–[12], [14]–[19]. Under this perspective, HANDEXOS was conceived in order to be a novel device. First, a shell-like structure was used for its links, on both the dorsal and the palmar side of the hand, in order to minimize the overall size of the device. This solution also provides a wide, distributed, and comfortable physical human–robot interface (pHRI). Second, a remote underactuation solution with a Bowden cables transmission was implemented to further reduce the inertia of the moving parts. Moreover, HANDEXOS has a number of active and passive DOFs sufficient to enable complete finger mobility (i.e., flexion and extension and abduction/adduction), provide nearly full range of motion (ROM), and allow for an adjustable size to comply with intersubject anthropometric variability. Finally, HANDEXOS and its actuation were conceived by considering the main deficits affecting the stroke hand (e.g., spasticity and the low capability of fingers extension [24], [25]) and the required rehabilitative therapy, which consists of driving repetitive tasks of fingers extension [24].

The organization of this paper is illustrated as follows. Section II describes the mechanics of the finger modules. Section III presents the actuation unit and Section IV focuses on the mechanical simulations carried out in order to support the design phase. Section V describes the sensory and control systems. Section VI reports the results of the experimental characterization of the HANDEXOS index module, and the experimental evaluation of the HANDEXOS dynamic model. Finally, results are discussed in Section VII and conclusion is drawn in Section VIII.

II. Mechanical Design

The concept of HANDEXOS [26] counts five independent modules [see Fig. 1(a)], one for each human finger. Each module is made of three links, with a shell-like structure, which fits the dorsal side of the user's phalanges [see Fig. 2(a), (b)]. Three additional orthotic shells, in contact with the palmar side of the finger, house three force sensors, one for each phalanx, in order to monitor the human/exoskeleton interaction forces (see Section V). Dorsal and palmar shells are fastened together by means of Velcro straps.

The links are connected with each other by means of active and passive DOFs. There are three active DOFs. One active DOF assists the extension/flexion of the human MCP joint [namely 2 in Fig. 2(a) and (b)]. It consists of a slider-crank-like mechanism [see detail in Fig. 2(c)] that, on one hand, allows the indirect transmission of the torque on the human MCP joint, on the other hand minimizes the undesired translational force caused by the misalignment between human-exoskeleton rotational axes (see Section VI). Other two active DOFs allow the assistance of the extension/flexion of the proximal interphalangeal (PIP) and distal interphalangeal (DIP) joints [namely 4 and 5 in Fig. 2(a), (b)].

Furthermore, there are three passive DOFs: one rotational and two translational joints. The rotational joint [namely 1 in Fig. 2(a) and (b)] allows for the human MCP abduction/adduction. One of the passive translational joint is between the HANDEXOS MCP and PIP joints [namely 3 in Fig. 2(a)

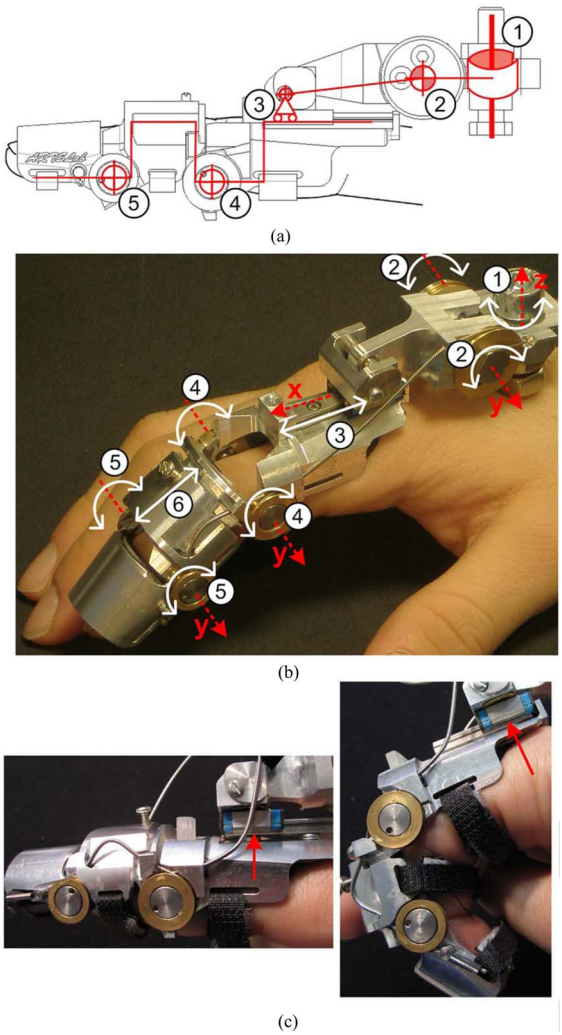

Fig. 2. (a) Kinematic layout of the HANDEXOS finger module. (b) Each finger module was provided with active and passive DOFs: (1) passive MCP abduction/adduction; (2) active MCP flexion/extension; (3) passive translational joint for torque transmission to the MCP joint; (4) active PIP flexion/extension; (5) active DIP flexion/extension and; (6) passive translational joint to adjust the intermediate link's length. (c) Detail of the proximal-link mechanism for the extended (on the left) and flexed (on the right) configurations.

and (b)]. It allows the setting of the relative distance between MCP and PIP joints according to the user's hand anthropometry. However, it is also part of the slider-crank-like mechanism. The second passive translational joint [namely 6 in Fig. 2(b)] is used to adjust the length of the HANDEXOS link coupled with the intermediate phalanx. This passive DOF results because the intermediate link is constituted of two reciprocally sliding concentric shells and allows for fitting the user specific PIP–DIP joint interaxes distance in the range 23–33 mm. This DOF is then blocked by means of a screw after the user wears the device [see Fig. 2(b)].

A soft layer of 3 mm of Neoprene foam (555XEB/3, M.T.O., Italy) covers the inner surface of the dorsal shells of the links. This soft layer provides a comfortable pHRI and allows for small adjustments between HANDEXOS and the human finger. A wrist orthopedic tutor fixes the finger and the palm modules to the user's hand.

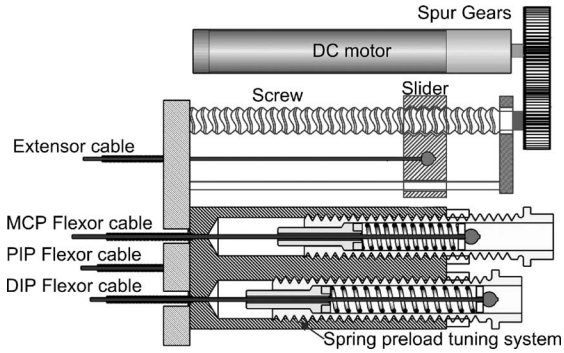

Fig. 3. Actuation unit: at the top the extension unit made of the motor connected by gears to a screw and to the slider that pulls the extension cable; at the bottom the flexion unit made of three passive compression springs, each one connected, through a cable, to a single joint. Note that in figure two of the three springs preload mechanisms are clearly visible that allow us to increase the springs preload if unscrewed.

In order to evaluate the mechanical design and the application of the HANDEXOS concept, we first developed modules for the index and middle fingers. It is important to point out that, with the exception of the thumb, all HANDEXOS finger modules have the same working principle and mechanical design. This paper is, therefore, concentrated on the characterization of the index finger module.

III. Actuation System

The HANDEXOS actuation system was designed in order to be light weight, modular, simply reconfigurable, and remotely located with respect to the hand. It is composed of an actuated extension unit and a passive flexion module (see Fig. 3).

The transmission system is based on steel wire ropes routed through spiral-spring Bowden cables (external diameter 1.6 mm, internal diameter 0.8 mm, Asahi Intecc, Japan). Although a Bowden cable introduces Coulomb friction, which causes a loss in the transmitted force, makes it possible to remotely locate the bulky actuation, and consequently, to reduce the total inertia of the wearable and moving parts [27].

The experience of our research group in the field of underactuated hand prostheses [28]–[30] suggested us to adopt similar design principle also for the HANDEXOS driving unit. Underactuation is a bioinspired solution to assist the hand rehabilitation. Although it does not allow the independent control of each joint, it simplifies the mechanism and requires a few control variables.

A. Extension Unit

For each finger of HANDEXOS, a single actuator drives the extension of the MCP, PIP, and DIP joints. The finger module is extended by a 0.6-mm nylon-coated steel cable wrapped around three idle pulleys placed in correspondence of each finger flexion/extension joint on one side of the exoskeleton finger [see Fig. 2(b)]. Then, the cable is fixed to the distal phalanx through a cable stop. The tendon cable is pulled by a linear slider driven by a dc motor (CR 18.10 W, Faulhaber, Germany) through a planetary gear with a reduction

ratio of 43 (series 23/1, Faulhaber, Germany). The motion is transmitted to a lead screw (pitch 0.5 mm) by means of spur gears (see Fig. 3).

B. Flexion Unit

The flexor unit consists of three antagonist cables, one for each joint of the finger module (see Fig. 3). Each cable is wrapped around each of the three flexion pulleys, which are placed on the opposite side of the finger module with respect to the extension pulleys [see Fig. 2(b)]. The flexion cables are then connected to three passive compression springs that allow for finger flexion when no voluntary action (or even caused by spasticity) is performed by the subject.

Such springs are housed in an aluminum case, remotely located in the actuation block. Compression springs preload can be easily regulated by means of three preload screw-driven tuning systems (see Fig. 3).

IV. Mechanical Simulations

Once defined the layout of HANDEXOS mechanics and actuation, we developed a dynamic model of the HANDEXOS finger module coupled with the human finger. This model was used to both size the actuation unit in terms of speed/torque requirements and transmission ratio and identify a set of suitable values for: joint pulleys radius and compression springs stiffness and preload.

A. Dynamic Model

We focused the analysis on the dynamics of the human finger when wearing HANDEXOS, considering the effect of the exoskeleton's driving torques on the human finger articulations. For sake of simplicity, we simulated the finger extension/flexion in the sagittal plane, while we assumed constrained the abduction/adduction motion.

Under these conditions, dynamics of the human finger is described by the following equation:

$$B(q)\ddot{q} + C(q,\dot{q})\dot{q} - F_v\dot{q} + g(q) = -\tau + Kr(x_0 - qr)\xi_F + J_1^T(q)H_1(q) + J_2^T(q)H_2(q) + J_3^T(q)H_3(q) \quad (1)$$

where $q, \dot{q}, \ddot{q}$ denote, respectively, the (3×1) human finger joint position, velocity, and acceleration vectors (q_1, q_2, q_3 are the human finger MCP, PIP, and DIP joints angle, respectively); $B(q)$ and $C(q,\dot{q})$ are, respectively, the (3×3) inertia matrix and the (3×3) matrix of centrifugal and Coriolis torques (these matrixes take into account the inertia and masses of both the finger and HANDEXOS links); F_v is the (3×3) diagonal matrix of viscous friction coefficients of the system HANDEXOS/finger; g is the (3×1) gravity vector; τ is the (3×1) vector of the actuation torques applied by the HANDEXOS extensor tendon to the human joints; $kr(x_0 - qr)\xi_F$ is the (3×1) vector of the torques applied by the flexor tendons connected to the compression springs to the human joints, where K is the (3×1) vector of the springs stiffness coefficients; x_0 is the (3×1) vector of the springs preloads; r is the (3×1) vector of the exoskeleton's pulley radii and ξ_F is the (3×1) force-transmission efficiency factor due to Bowden cables friction losses; H_i is the (6×1) vector of forces and moments deriving from the human/exoskeleton interaction (including any possible muscular action) and J_i is the (6×3) matrix of geometric Jacobian evaluated in the forces application points.

The agonistic action for the extension of the finger module is driven by the cable tension T. In absence of friction, T could be assumed constant along the whole path of the cable. Unfortunately, when the tendon is routed through multiple Bowden segments, it is necessary to take into account the friction losses. As described in [31], such losses can be modeled as an efficiency factor ξ, coupling the force at the two Bowden cable extremities (T_1 and T_2) as in the following:

$$T_1 = T_2\xi \quad (2)$$

$$\xi = e^{\mathrm{sgn}(v)\mu\gamma} \quad (3)$$

where μ is the friction coefficient between the steel cable and the inner layer of the Bowden cable, v is the sliding velocity of the cable inside the Bowden cable, and γ is the bending angle along the transmission.

For HANDEXOS, assuming the steel cable infinitely stiff, the friction losses along the path of the extension cable are described by the following equations:

$$T = T_1\xi_{1E} \quad (4)$$

$$T_1 = T_2\xi_{2E} \quad (5)$$

$$T_2 = T_3\xi_{3E} \quad (6)$$

where

$$\xi_E = [\xi_{1E}\ \xi_{2E}\ \xi_{3E}]^T = [e^{\mathrm{sgn}(\dot{q}_1)\mu\gamma_1}\ e^{\mathrm{sgn}(\dot{q}_2)\mu\gamma_2}\ e^{\mathrm{sgn}(\dot{q}_3)\mu\gamma_3}]^T \quad (7)$$

is the vector containing in rows the force transmission efficiency, respectively, for path $1E$, $2E$, and $3E$ of the extensor tendon cable [see Fig. 4(a)].

So, considering the schematic representation reported in Fig. 4(b), and (4)–(7) the extension torques generated on each finger joint by the cable tension T are

$$\tau = \begin{pmatrix} \tau_1 \\ \tau_2 \\ \tau_3 \end{pmatrix} = \begin{pmatrix} \dfrac{Tr_1\xi_{1E}}{l_1\cos(q_1 - \theta_1)} \cdot \dfrac{l_1\cos\theta_1 - h\sin q_1}{\cos q_1} \\ T\xi_{1E}\xi_{2E}r_2 \\ T\xi_{1E}\xi_{2E}\xi_{3E}r_3 \end{pmatrix} \quad (8)$$

where τ_1 is the torque deriving from the action of the cable tension on the HANDEXOS MCP joint and transmitted to the human MCP articulation through the slider-crank-like mechanism. Further θ_1 is the HANDEXOS MCP angle that is a function of the human MCP angle q_1 [see Fig. 4(b)]

$$\theta_1 = q_1 + \sin^{-1}\left(\frac{d\cos q_1 - b\sin q_1 - h}{l_1}\right) \quad (9)$$

where l_1 (0.035 m) is the length of the slider-crank-like mechanism link, d (0.024 m) is the vertical distance between the exoskeleton and human MCP joint, h (0.007 m) is the distance between the translational axis of the slider and the proximal link, and b is the horizontal shift between the human and the

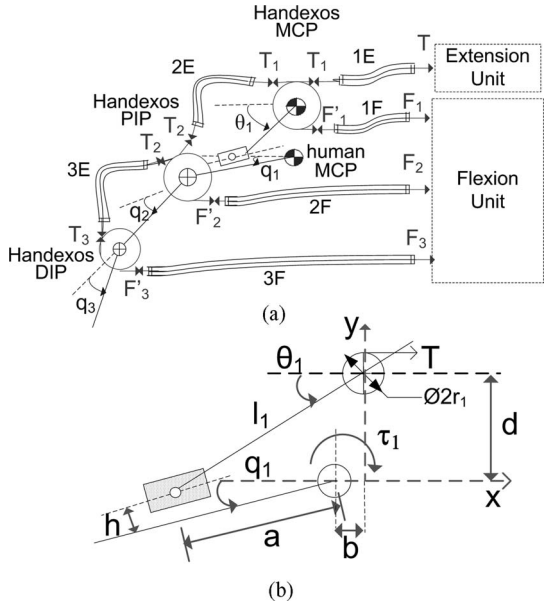

Fig. 4. (a) Schematic representation of the agonistic and antagonistic Bowden cable transmission system. The extension tension T and each flexion springs force (here represented as F_1, F_2, F_3) are damped by friction losses through each Bowden path so that $T_i = T_{i+1}\xi_{(i+1)E}$ and $F_i = F_i'\xi_{iF}$. (b) Detail of the proximal link mechanism.

exoskeleton MCP rotational axes. We assumed b equal to zero since all subjects worn HANDEXOS by attempting to minimize it.

The same considerations about the friction losses due to the Bowden cables are then applied to the three flexion cables [see Fig. 4(a)]. The efficiency factor is accordingly defined

$$\xi_F = [\xi_{1F}\ \xi_{2F}\ \xi_{3F}]^T = [e^{-\mathrm{sgn}(\dot{q}_1)\mu\gamma_1}\ e^{-\mathrm{sgn}(\dot{q}_2)\mu\gamma_2}\ e^{-\mathrm{sgn}(\dot{q}_3)\mu\gamma_3}]^T \quad (10)$$

where the elements in rows, respectively, refer to the paths $1F$, $2F$, and 3F between the flexion unit and the MCP, PIP, and DIP joints [see Fig. 4(a)].

B. Results of the Simulations

We implemented equations (1)–(10) in MATLAB, by assuming the following set of parameters for the mass m_i, the inertia I_i, and the length n_i of each human/exoskeleton link: $m_1 =$ 0.05 Kg, $m_2 =$ 0.039Kg, and $m_3 =$ 0.031 Kg; $I_1 = 85.8 \times 10^{-6}$ Kg. m^2, $I_2 = 4 \times 10^{-6}$Kg. m^2, and $I_3 = 2.4 \times 10^{-6}$ Kg. m^2; $n_1 =$ 0.051m, $n_2 =$ 0.025 m, and $n_3 =$ 0.026 m. Mass, inertia, and length of human phalanges were calculated through the GeBOD Anthropometric Database (accessible through the ADAMS software) for a standard man (75 Kg, 1.80 m tall). Mass, inertia, and length of each HANDEXOS link, instead, were calculated from the HANDEXOS 3-D CAD design. Human finger joints viscosity was estimated to be equal to $F_v =$ 0.005 [32]. For friction losses accounted by (7) and (10), being the inner layer of the Bowden cables covered by stainless steel, we assumed the kinetic friction coefficient μ equal to 0.57 [33]. The bending angles γ, instead, vary with the spatial configuration that the Bowden cables assume during the experimental trials. In order to estimate a value of the bending angles, for the aim of the simulation, we hypothesized a scenario that we then recreated for the experimental activities reported in Section VI. In particular, being paths $2E$ and $3E$ [see Fig. 4(a)] univocally determined by mechanical constraints [see Fig. 2(b)], we assumed their bending angles γ constant over trials and among subjects, and equal to π and 0.5 radians, respectively. Instead, being paths $1E$, $1F$, $2F$, and $3F$ [see in Fig. 4(a)] dependant on the relative position of the actuation unit and the finger module, we assumed to fix the spatial location of the actuation unit so that the bending angles measure 0.1 for $1E$ and π/2, 0.2, 0.1 for $1F$, $2F$, and $3F$, respectively. Once defined the bending angles, we estimated the efficiency factors as following: $\xi_{1E} = 0.41$, $\xi_{2E} = 0.20$,$\xi_{3E} = 0.75$; $\xi_{1F} = 0.89$, $\xi_{2F} = 0.94$, and $\xi_{3F} = 0.94$.

Being the model completely described, a simulated task of finger extension/flexion driven by HANDEXOS has been simulated in MATLAB in order to: 1) identify a set of suitable values for pulleys radii (r_i), compression springs stiffness (K_i), and preloads (x_{0i}); 2) size the actuation unit in terms of dc motor power, spur gears and motor gear transmission ratio, and lead screw pitch. In particular, we simulated the task in a borderline case in order to consider the most demanding situation for the actuation unit. For this purpose, we considered a prototypical extension/flexion trajectory having duration of 5 s (i.e., 2.5 s for extension and 2.5 s for flexion) as recorded from healthy subjects during grasping in [34]. So, we iteratively modified r_i, K_i, and x_{0i} until we achieved a minimum error between the simulated and the reference joint trajectories, starting from a set of values matching the initial and final prototypical static postures. During the simulation, we considered a 10-N constant force acting between each exoskeleton and human phalanx, and perpendicularly to the finger–phalanx longitudinal direction. Such a value for the opposing force was considered a borderline case accordingly to the physicians and therapists who collaborated with us in this work. From the simulations we got the following design parameters: $r_1 =$ 0.009 m, $r_2 =$ 0.006 m, $r_3 =$ 0.005 m; $K_1 =$ 590 N/m, $K_2 =$ 590 N/m, $K_3 =$ 590 N/m; $x_{01} =$ 0.040 m, $x_{02} =$ 0.050 m, $x_{03} =$ 0.018 m. In addition, simulations pointed out that achieving the execution of the prototypical task would require a maximum tendon cable force of about 150 N with the slider speed being equal to 6 mm/s. These considerations led to the actuation unit described in Section III-A.

V. Sensory and Control System

A. Sensors

The HANDEXOS sensory system comprises a number of sensors embedded both in the exoskeleton and in the actuation unit. An incremental magnetic encoder (HEDS-5540 A, Faulhaber, Germany) is hinged on the motor axis. Three force sensors are mounted on the surface of the inner side of each of the three palmar shells in order to sense the interaction force at the palmar side [see Fig. 5(a)]. The force sensors are commercial piezoresistive silicon sensors (operating force 0–15 N, sensitivity 0.012 V/N, FSS1500NSB, Honeywell, FS Series, NJ). Two Hall sensors (A3213, Allegro MicroSystems, Inc., MA) are housed along the screw to work as limit switches [see

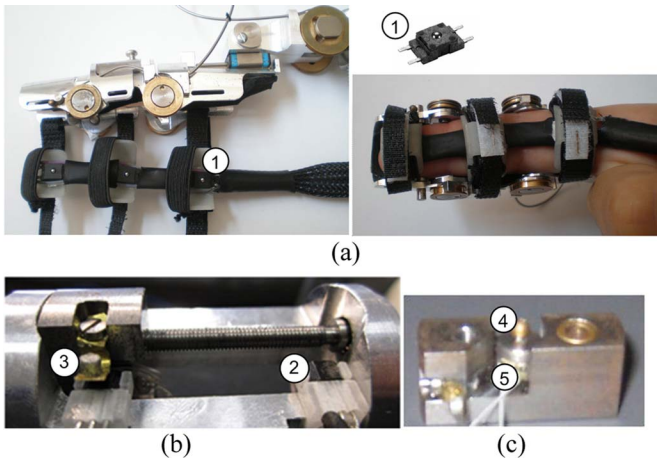

Fig. 5. (a) HANDEXOS shells equipped with three force sensors (1). (b) Extension unit equipped with two Hall sensors (2) that perceive the magnetic field generated by the magnet (3). (c) Cable tension sensor (5) made of strain gauges. It is mounted on a microfabricated cantilever structure on which the cable stop acts (4).

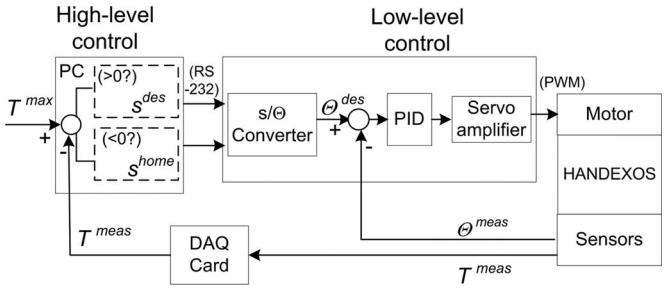

Fig. 6. Control flow diagram of the HANDEXOS system.

Fig. 5(b)]. The linear slider is equipped with strain gauges [see Fig. 5(c)] to sense the force transmitted by the driving cable (operating range: 0–120 N; resolution 20 mN) [30].

B. Control System

HANDEXOS is controlled by means of a hierarchical control system (see Fig. 6). A low-level layer, running at 5 kHz on a standalone motion controller, implements the position control of the linear slider, which is a classical PID closed-loop regulator with an antiwindup scheme. The PID solution was selected to compensate for the external force applied by the end users against the HANDEXOS extension action and to guarantee zero-error at steady state. The PID parameters were tuned by means of a standard Ziegler–Nichols method. The selected parameters allows for a 10-Hz closed-loop bandwidth and null overshoot step response. The motion controller reads the motor encoder Θ^{meas} and the limit switches and drives the motor to the desired position Θ^{des} by means of a pulsewidth modulation-based custom-made current servo amplifier. A high-level layer, running on a remote PC at 100 Hz, sets the desired position of the linear slider s^{des} in accordance with the rehabilitative task to be performed.

The high level layer is also responsible for monitoring the cable force and for reverting the slider motion in the case of force overload $T^{\mathrm{meas}} > T^{\max}$, i.e., high-level control drives the motor to reach the configuration s^{home} corresponding to a full-flexed finger posture. This has been designed in order to face the unexpected situations in treating with real patients (e.g., high resistance or uncontrolled motion given by a spastic user).

The force threshold was set to $T^{\max} = 150$ N. This value was chosen because it allows a maximum torque on HANDEXOS MCP joint of 1.3 Nm, and a maximum undesired translational force transferred on the human MCP joint by the slider-crank-like mechanism of 40 N, the latter being compatible with the range of reaction forces acting on human MCP joint while performing activities of daily living [35]. This allows it to rely upon a safety control loop that makes it possible to prevent injuries in the case of hand's spasmodic motion.

VI. Experimental Characterization

HANDEXOS experimental characterization was aimed at achieving three objectives: 1) to assess that wearing HANDEXOS does not modify significantly finger extension/flexion kinematics; 2) to evaluate the amount of undesired translational force acting on human MCP joint as a consequence of human–robot joint axes misalignment; and 3) to assess the accuracy of the dynamic model described in Section IV.

A. Comparison of Finger Kinematics With and Without Wearing HANDEXOS

In this first experiment, we compared human finger joint trajectories while performing a prototypical extension/flexion task with and without wearing HANDEXOS. Five healthy subjects participated in the experiments (3 males and 2 females), after they provided their informed consent. Each subject performed a prototypical extension/flexion task in two different modes: 1) subjects actively performed the finger extension/flexion without wearing the exoskeleton, i.e., "no exoskeleton" (NE) mode; 2) subjects worn HANDEXOS that was programmed to extend their index finger while they were instructed to stay as passive as possible, i.e., "no action" (NA) mode. In NA mode, each subject repeated five times the prototypical rehabilitation task, having duration of about 20 s (i.e., 10 s for extension and 10 s for flexion) [24]. In NA mode, the same task was driven by moving back and forth the HANDEXOS linear slider at a constant speed of 1.2 mm/s. In both NE and NA modes, finger joints trajectories were recorded (sampling frequency of 100 Hz) by means of a motion capture system (460, VICON, Oxford, U.K.).

It is worth noting that before starting the experiments, we set the equilibrium positions of the compression springs at $x_{01} = 0.001$ m, $x_{02} = 0.006$ m, and $x_{03} = 0.002$ m, which were estimated by the dynamic model to be the right preload for the characteristics of the current task and the specific case of null or very low opposing force, as we expected from healthy volunteers. Indeed, normal subjects exerted null (in NA mode) or much lower forces (in OA mode, see Section VI-C) than the borderline case considered for an appropriate sizing of the actuation unit.

For sake of simplicity, we reported the graphical results for one out five subjects. In particular trajectories for Subject #1 in NA and NE modes, averaged over five repetitions, are shown in

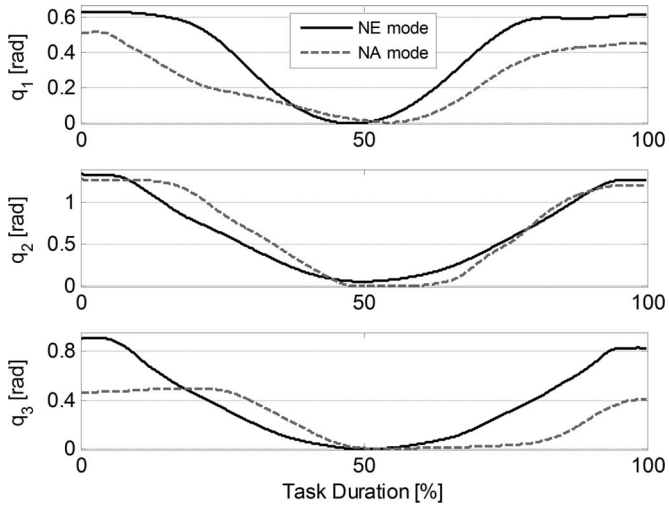

Fig. 7. Human MCP, PIP, and DIP trajectories acquired during NA (dashed line) and NE (solid line) modes for subject #1.

TABLE I
PEARSON PRODUCT MOMENT CORRELATION AVERAGED OVER FIVE REPETITIONS FOR EACH SUBJECT

	Subj. #1	Subj. #2	Subj. #3	Subj. #4	Subj. #5
r_p (q_1)	0.8851	0.8080	0.7070	0.7407	0.9316
r_p(q_2)	0.9598	0.7657	0.9819	0.9047	0.8998
r_p (q_3)	0.7023	0.5470	0.8714	0.5482	0.6282

Fig. 7. For each subject and repetition, the level of similarity of joint trajectories between NE and NA modes was assessed by calculating the Pearson product moment correlation r_P. Table I reports the values of r_P averaged over the five repetitions for all subjects. Over five subjects, the mean value (along with its standard deviation) of r_P is equal to 0.81 $\pm$ 0.09, 0.91 $\pm$ 0.08, and 0.66 $\pm$ 0.2, respectively, for MCP, PIP, and DIP joint trajectories.

B. Evaluation of Undesired Translational Force on Human MCP Articulation

In this section, we exploited data collected in NA mode to evaluate the amount of undesired translational force loading human MCP articulation as a consequence of human–robot MCP joint axes misalignment. Because of the complexity of a direct measurement of such undesired translational force, we estimated it through a static analysis of the HANDEXOS proximal slider-crank-like mechanism. We could neglect dynamics effects being the prototypical task quite slow. By analyzing the static equilibrium of the slider-crank-like mechanism [see Fig. 4(b)] and taking into account (8)–(9), the maximum undesired translational force R in its components x and y (refer to Fig. 4 for the axes of reference) acting on human MCP joint as a consequence of tension cable T is equal to

$$R_{1x} = \frac{Tr_1}{l_1 \cos(q_1 - \theta_1)} \sin q_1 \tag{11}$$

$$R_{1y} = \frac{Tr_1}{l_1 \cos(q_1 - \theta_1)} \cos q_1 . \tag{12}$$

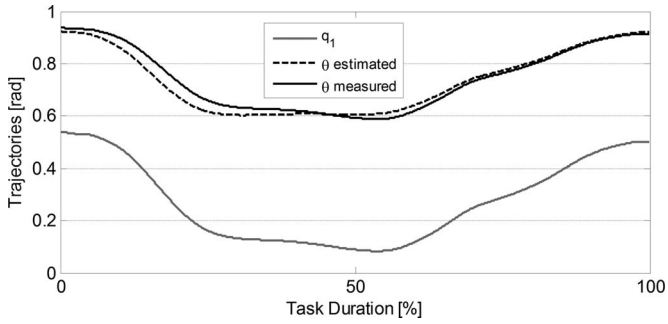

Fig. 8. Acquired (θ_1 in solid black line) and estimated ($\hat{\theta}_1$ in dashed black line) HANDEXOS MCP trajectories for subject #2. The gray line represents the human MCP trajectory q_1.

TABLE II
AVERAGE AND STANDARD DEVIATION OF RMS AND MAX ERR FOR EACH SUBJECT

	Subj.1	Subj.2	Subj.3	Subj.4	Subj.5
RMS [rad]	0.033± 0.02	0.026± 0.04	0.030± 0.05	0.023± 0.04	0.034± 0.05
Max Error [rad]	0.065± 0.06	0.023± 0.05	0.066± 0.07	0.031± 0.04	0.065± 0.06

It is worth noting that, for a certain value of T, (11) and (12) give an estimate of R in the worse scenario of zero force exerted by the flexor unit counterbalancing the force applied by the extensor cable on HANDEXOS MCP pulley.

Being known both human and HANDEXOS MCP joint trajectories by means of the motion tracking system, and having measured T (maximum T was equal to 34.48 N) we estimated the upper boundaries for R_{1x} and R_{1y} as follows:

$$R_{1x} \leq 2.05\,\mathrm{N} \tag{13}$$

$$R_{1y} \leq 7.41\,\mathrm{N}. \tag{14}$$

In addition to the earlier estimate of the upper boundaries for R, we assessed the amount of such undesired translational force by also evaluating its consequent effect in terms of reciprocal translation of the HANDEXOS with respect to the human hand. Indeed, being the coupling between the user's hand and the device not perfectly rigid, any translational force acting on the MCP human joint can cause the HANDEXOS palmar module to slide off. In the hypothesis that the undesired translational force is null, human MCP joint q_1 and HANDEXOS MCP joint θ_1 are linked by a fixed mathematical relation, as shown in (9) (i.e., θ_1 can be estimated from q_1). Therefore, whenever a reciprocal translation exists, (9) is not more valid, thus θ_1 is badly estimated from q_1. In such a way, it is possible to evaluate the amount of the undesired reciprocal translation in terms of difference between the measured (i.e., θ_1) and the estimated through (9) (i.e., $\hat{\theta}_1$) HANDEXOS MCP joint postures, being known the correspondent human joint trajectory q_1.

Fig. 8 compares (for Subject #2) the measured q_1 and θ_1 angles with $\hat{\theta}_1$. Difference between measured and estimated HANDEXOS MCP joint trajectories was quantified by computing the rms and the maximum value of $(\hat{\theta}_1 - \theta_1)$, as reported in Table II for each subject. The calculated values, respectively,

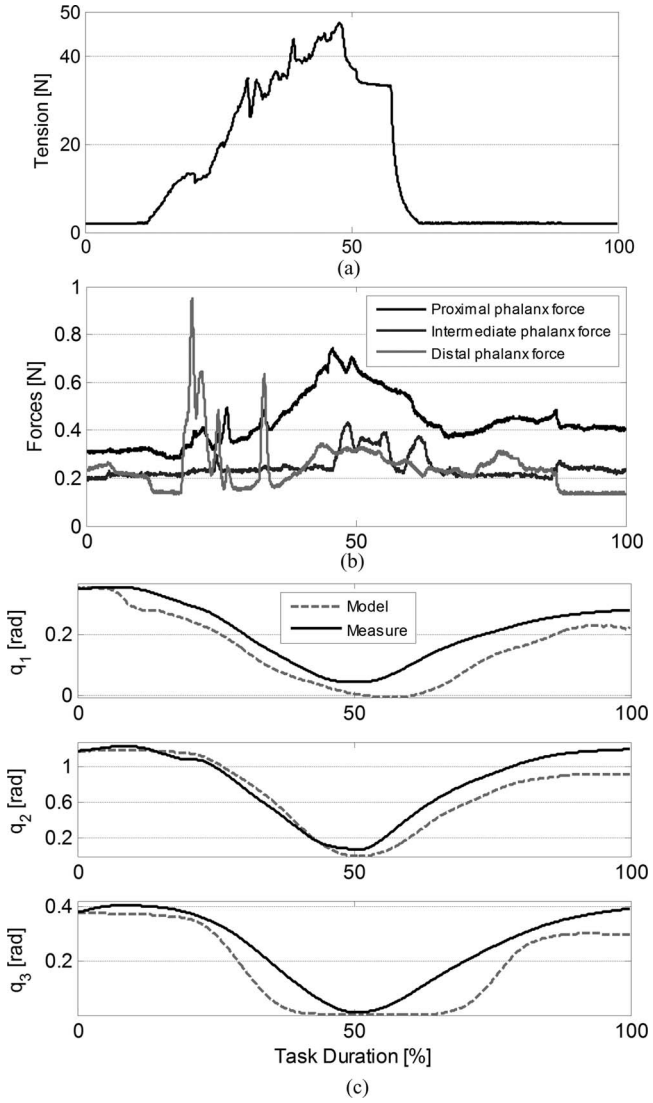

Fig. 9. (a) Cable tension measured in OA mode for subject #1. (b) Proximal, intermediate, and distal interaction forces measured during the extension/flexion task in OA mode for subject #1. (c) Details on the accuracy of the dynamic model for MCP, PIP, and DIP trajectories for subject #1.

spanned in the range of 0.023–0.034 and 0.023–0.065 rad, corresponding to a maximum translation d in the range of 1–1.3 mm, or a maximum translation s in the range of 1–3.6 mm.

C. Validation of the Dynamic Model

In this section, we validated the dynamic model described in Section IV. Since the model was developed by considering the opposing action that stroke patients could exert, we validated the model accuracy in a similar condition. Indeed, the same five subjects were asked to repeat five times the extension/flexion task as in NA mode, while exerting a slightly opposing force against the HANDEXOS extension action, i.e., "opposing action" (OA) mode.

In order to validate the accuracy of the dynamic model we run simulations by using the following collected data: cable tension and interaction forces (see in Fig. 9(a) and (b) a recording for Subject #1), and the initial values of q, $\dot{q}$, and $\ddot{q}$. In addition, for each subject, we estimated phalanges masses and inertias, through the GeBOD database. Measured and simulated trajectories are shown in Fig. 9(c) for subject # 1.

TABLE III
PARAMETERS DESCRIBING THE ACCURACY OF THE DYNAMIC MODEL VALIDATED WITH FIVE DIFFERENT SUBJECTS AND AVERAGED OVER FIVE REPETITIONS

		Subj.1	Subj.2	Subj.3	Subj.4	Subj.5
Final q_1	*(Mod)*	0.28	0.25	0.26	0.38	0.36
	(Meas)	0.23	0.16	0.31	0.29	0.32
Final q_2	*(Mod)*	1.19	0.84	0.73	0.86	0.92
	(Meas)	0.91	0.74	0.79	1.15	1.20
Final q_3	*(Mod)*	0.39	0.31	0.20	0.24	0.29
	(Meas)	0.31	0.51	0.25	0.32	0.24
Min q_1	*(Mod)*	0.04	0.003	0.095	0.12	0.04
	(Meas)	-0.004	0.003	0.085	0.13	0.006
Min q_2	*(Mod)*	0.081	-0.025	0.18	0.18	0.12
	(Meas)	0.002	-0.06	0.061	0.05	0.19
Min q_3	*(Mod)*	-0.01	0.11	-0.003	0.008	-0.016
	(Meas)	0.004	-0.019	0.03	-0.006	0.029
R^2 (q_1)		0.92	0.89	0.75	0.75	0.86
R^2 (q_2)		0.92	0.92	0.79	0.78	0.87
R^2 (q_3)		0.71	0.82	0.87	0.93	0.85

All angles are reported in radians.

In order to assess the accuracy of the dynamic model we compared, for each finger joint, the measured q_i and simulated by the model $\hat{q}_i$ trajectories in terms of: final and minimum values of joint angles, and R^2 coefficient (R^2, defined as the square of the correlation coefficient between q_i and $\hat{q}_i$).

Table III reports, for each subject, the averaged (over five repetitions) value of measured and simulated final and minimum joint angles, along with the R^2 coefficient whose values were in the range of 0.71–0.93.

VII. DISCUSSION

This paper introduced the mechatronic design and development of HANDEXOS finger module. Extensive experimental activities were conducted involving five healthy subjects in order to: 1) assess the HANDEXOS wearability, its capability to fit intersubjects anthropometric variability and its effect on the user's finger extension/flexion kinematics; 2) assess the undesired translational force loading human MCP joint as a consequence of the HANDEXOS-user MCP joint axes misalignment; and 3) evaluate the accuracy of the proposed dynamic model and its usability to properly set the flexion unit preload on the basis of the amount of opposing force applied by subjects.

First, experimental characterization pointed out that all five subjects could easily wear HANDEXOS and successfully perform extension/flexion tasks in both NA and OA modes. Indeed, thanks to its passive DOFs, HANDEXOS could fit the hand anthropometry of each subject, and none of them reported any discomfort in wearing the device.

Second, comparing trajectories collected in NE and NA modes showed that HANDEXOS allowed for an anthropomorphic kinematics. Indeed, as demonstrated in Fig. 7 for Subject #1 and confirmed by data recorded from the other subjects, only slight differences between NE and NA modes were evident. The first difference consists in the extension time of the MCP joint that is, on average, 1.4 s shorter during NA mode. This behavior is a consequence of a suboptimal choice for the MCP compression spring stiffness (lower than necessary). The second difference was that finger joints ROM was wider in NE than in NA mode, especially for the DIP joint ($\Delta q_3 = 0.4 \pm 0.1$ rad). This difference was caused by the limited stroke ($\Delta s = 0.018$ m) of the linear slider used in the current version of the actuation unit that needs to be optimized (needed $\Delta s = 0.025$ m).

By discussing on how to improve kinematics similarity, it is worth noting that, in an underactuated system, the finger extension/flexion dynamics depends on a number of parameters that is higher than the actual number of control variables. Indeed, while we can solely drive the extensor tendon cable (i.e., our control variable), dynamics is influenced by three compression springs preload and the opposing force vectors exerted by the subject acting on each HANDEXOS link. Nevertheless, this well-known drawback of underactuation [36] does not affect the HANDEXOS usability as a rehabilitation tool. We expect that in the real application scenario involving stroke patients, given a certain amount of opposing force, we can set a preload that allows HANDEXOS to complete the rehabilitative task. On the other hand, underactuation offers the great advantage to place remotely the actuation unit and to simplify a lot both the actuation and control system. This makes the device less bulky and easy to be accepted by users, as well as more portable.

Third, the estimate of undesired translational force generated by the wearable device in NA mode on the MCP joint (see Fig. 8 and Table II) pointed out that HANDEXOS does not overload MCP articulation more than activities of daily living can do [35]. On one hand, the theoretical estimate of R through (11) and (12) indicated an upper boundary for the absolute value of $R < 10$ N. On the other hand, a small (only a few millimiters) reciprocal motion between HANDEXOS palm and human hand metacarpus was indirectly measured. Moreover, although this computation was done only in NA mode, HANDEXOS control system is endowed with a safety loop that limits the maximum extensor tendon cable force to 150 N and as a consequence to 40 N the maximum absolute value for R. Finally, we validated the dynamic model exploiting data collected in OA mode with healthy volunteers. All the subjects exerted an opposing force lower than the borderline case of 10 N considered during the modeling phase in order to identify the most demanding situation for the actuation unit in terms of maximum torque to deliver. This happened because we asked the subjects to slightly oppose the motion while they neither receive any feedback nor any force reference about the force they actually exerted. This choice was voluntarily taken because, for the aim of the model validation, we did not need to consider the most critical condition. Rather, in this way, we could perform the validation while keeping simple the experimental setup.

Results reported in Fig. 9 and Table III motivate us to state that the dynamic model can successfully predict kinematic trajectories, being known initial conditions and the interaction force profiles. Indeed, the maximum error committed to predict the final joint position was of 0.28 rad (for q_2, Subject 4) which corresponds to 20% of the joint ROM, while on average this error was of 0.06 rad for q_1, 0.19 rad for q_2, and 0.09 rad for q_3, respectively, 12%, 15.7%, and 18% of q_1, q_2, and q_3 ROM. Moreover, R^2 was always higher than 0.7 (and equal to 0.84 on average) for all joints and all trajectories. These values are acceptable if we consider the difficulty in modeling Bowden cables [27], [31]. In fact, any significant error in modeling friction loss would significantly affect the capability of the model to predict finger postures. Prediction capabilities of the dynamic model can be exploited in real scenario applications both to online evaluate the effect of a certain springs preload on the dynamics of the system and to suggest an alternative setting in the case of a significant change of the opposing force over trials.

VIII. Conclusion

The aim of this paper was to present the mechatronic design of HANDEXOS and the preliminary characterization of the performance of its finger module.

The shells' structure and the underactuation solution make HANDEXOS a compact and light weight exoskeleton, with acceptable cosmetic appearance. Experiments demonstrated that it allows good and safe usability. Therefore, compared with other known hand exoskeletons, HANDEXOS represents a tradeoff between the need of a light weight device with a compact actuation block and the need of a wearable multiphalanges device with an anthropomorphic kinematics.

Even if HANDEXOS has been mainly conceived for post-stroke rehabilitation, in principle it can be exploited for other applications. Indeed, it has an intrinsic versatility in the design that allows us to modify its actuation/transmission system, accordingly to the specific application (from the underactuation to the independent joint actuations) [37].

Further development of this work will be devoted to the redesign of each finger module in order to reduce their overall dimension, to the use of nonmetallic materials, and to the improvement of the actuation unit by means of series-elastic actuation. The system will be exploited to analyze hand motor control strategies and to characterize the biomechanics of post-stroke hand. The crucial lack of knowledge in this field raised our interest in improving the knowledge of the underlying motor and control disturbance of a post-stroke hand toward an improved rehabilitation therapy.

Acknowledgment

The authors would like to thank Dr. C. Cipriani and M. Controzzi for help in constructing the experimental apparatus.

References

[1] D. Epstein, A. Mason, and A. Manca, "The hospital costs of care for stroke in nine European countries," *Health Econ.*, vol. 17, pp. S21–S31, 2008.

[2] R. Colombo, F. Pisano, S. Micera, A. Mazzone, C. Delconte, M. C. Carrozza, P. Dario, and G. Minuco, "Robotic techniques for upper limb evaluation and rehabilitation of stroke patients," *IEEE Trans. Neural Syst. Rehabil. Eng.*, vol. 13, no. 3, pp. 311–324, Sep. 2005.
[3] G. B. Prange, M. J. A. Jannink, C. G. M. Groothuis-Oudshoorn, H. J. Hermens, and M. J. IJzerman, "Systematic review of the effect of robot-aided therapy on recovery of the hemiparetic arm after stroke," *J. Rehabil. Res. Develop.*, vol. 43, no. 2, pp. 171–184, 2006.
[4] V. S. Huang and J. W. Krakauer, "Robotic neurorehabilitation: A computational motor learning perspective," *J. NeuroEng. Rehabil.*, no. 6, p. 5, 2009.
[5] C. D. Takahashi, L. Der-Yeghiaian, V. Le, R. R. Motiwala, and S. C. Cramer, "Robot-based hand motor therapy after stroke," *Brain*, vol. 131, pp. 425–437, 2008.
[6] O. Lambercy, L. Dovat, R. Gassert, E. Burdet, C. L. Teo, and T. Milner, "A haptic knob for rehabilitation of hand function," *IEEE Trans. Neural Syst. Rehabil. Eng.*, vol. 15, no. 3, pp. 356–366, Sep. 2007.
[7] L. Masia, H. I. Krebs, P. Cappa, and N. Hogan, "Design and characterization of hand module for whole-arm rehabilitation following stroke," *IEEE/ASME Trans. Mechatronics*, vol. 12, no. 4, pp. 399–407, Aug. 2007.
[8] M. Bouzit, G. Burdea, G. Popescu, and R. Boian, "The Rutgers Master II—New design force-feedback glove," *IEEE/ASME Trans. Mechatronics*, vol. 7, no. 2, pp. 256–263, Jun. 2002.
[9] H. C. Fischer, K. Stubblefield, T. Kline, X. Luo, R. V. Kenyon, and D. G. Kamper, "Hand rehabilitation following stroke: A pilot study of assisted finger extension training in a virtual environment," *Top Stroke Rehabil.*, vol. 14, pp. 1–12, 2007.
[10] T. Koyama, K. Takemura, and T. Maeno, "Development of an ultrasonic clutch for multi-fingered exoskeleton haptic device using passive force feedback for dexterous teleoperation," in *Proc. IEEE/RSJ Conf. Intell. Robots Syst.*, 2003, pp. 2229–2234.
[11] M. Fontana, A. Dettori, F. Salsedo, and M. Bergamasco, "Mechanical design of a novel hand exoskeleton for accurate force displaying," in *Proc. IEEE Int. Conf. Robot. Autom.*, Japan, 2009, pp. 1704–1709.
[12] P. Stergiopoulos, P. Fuchs, and C. Laurgeau, "Design of a 2-finger hand exoskeleton for VR grasping simulation," presented at the Eurohaptics Conf., Dublin, Ireland, 2003.
[13] Stanford University Exoskeleton. (2008). [Online]. Available: http://bdml.stanford.edu/twiki/bin/view/Haptics/HapticsPictures
[14] J. Blake and H. B. Gurocak, "Haptic glove with MR brakes for virtual reality," *IEEE/ASME Trans. Mechatronics*, vol. 14, no. 5, pp. 606–615, Oct. 2009.
[15] A. Wege and G. Hommel, "Embedded system design for a hand exoskeleton," in *Embedded Systems—Modeling, Technology, and Applications*. Netherlands: Springer-Verlag, 2006.
[16] S. Ito, H. Kawasaki, Y. Ishigure, M. Natsume, T. Mouri, and Y. Nishimoto, "A design of fine motion assist equipment for disabled hand in robotic rehabilitation system," *J. Franklin Inst.*, vol. 348, pp. 79–89, 2011.
[17] B. H. Choi and H. R. Choi, "SKK hand master," in *Proc. IEEE/RSJ Int. Conf. Intell. Robots Syst.*, 2000, pp. 1131–1136.
[18] Cybergrasp. (2000). [Online]. Available: http://www.vrealities.com/cybergrasp.html
[19] Utah/MIT Dextrous Hand. (1993). [Online]. Available: http://www.sarcos.com/interspec_ut_mithand.html
[20] L. Lenny, Y. Matsuoka, and M. DiCicco, "An EMG-controlled hand exoskeleton for natural pinching," *J. Robot. Mechatronics.*, vol. 16, pp. 482–488, 2004.
[21] M. Iwaki, Y. Hasegawa, and Y. Sankai, "Fingertip stiffness control using antagonistic pairs of polyarticular tendons drive system," in *Proc. IEEE Int. Conf. Robot. Biomimetics*, Guilin, China, 2009, pp. 925–930.
[22] A. Chiri, F. Giovacchini, N. Vitiello, E. Cattin, S. Roccella, F. Vecchi, and M. C. Carrozza, "HANDEXOS: Towards an exoskeleton device for the rehabilitation of the hand," in *Proc. IEEE/RSJ Conf. Intell. Robots Syst.*, St Louis, MO, 2009, pp. 1106–1111.
[23] A. H. A. Stienen, E. E. G. Hekman, F. C. T. Van Der Helm, and H. Van Der Kooij, "Self-aligning exoskeleton axes through decoupling of joint rotations and translations," *IEEE Trans. Robot.*, vol. 25, no. 3, pp. 628–633, Jun. 2009.
[24] J. A. De Lisa, B. M. Gans, W. L. Bockenek, W. R. Frontera, L. H. Gerber, S. R. Geiringer, W. S. Pease, L. R. Robinson, J. Smith, T. P. Stitik, and R. D. Zafonte, *Physical Medicine and Rehabilitation: Principles and Practice*. Hagerstown, MD: Lippincott Williams & Wilkins, 2004.
[25] D. G. Kamper, H. C. Fisher, E. G. Cruz, and W. Z. Rymer, "Weakness is the primary contributor to finger impairment in chronic stroke," *Arch. Phys. Med. Rehabil.*, vol. 87, pp. 1262–1269, 2006.
[26] "Wearable mechatronic device," International Patent (pending) PCT/IB2008/001990; "Ortesi meccatronica per la mano," Italian Patent PI2007A000088.
[27] N. Vitiello, T. Lenzi, S. M. M. De Rossi, S. Roccella, and M. C. Carrozza, "A sensorless torque control for antagonistic driven compliant joints," *Mechatronics*, vol. 20, no. 3, pp. 355–367, 2010.
[28] M. C. Carrozza, G. Cappiello, S. Micera, B. B. Edin, L. Beccai, and C. Cipriani, "Design of a cybernetic hand for perception and action," *Biol. Cybern.*, vol. 95, no. 6, pp. 629–644, 2006.
[29] C. Cipriani, M. Controzzi, and M. C. Carrozza, "Objectives, criteria and methods for the design of the SmartHand transradial prosthesis," *Robotica*, vol. 28, pp. 919–927, 2010.
[30] M. C. Carrozza, B. Massa, S. Micera, R. Lazzarini, M. Zecca, and P. Dario, "The development of a novel prosthetic hand-ongoing research and preliminary results," *IEEE/ASME Trans. Mechatronics*, vol. 7, no. 2, pp. 108–114, Jun. 2002.
[31] A. Schiele, P. Letier, R. Van Der Linde, and F. Van Der Helm, "Bowden cable actuator for force feedback exoskeletons," in *Proc. IEEE/RSJ Int. Conf. Intell. Robots Syst.*, Beijing, China, 2010, pp. 3599–3604.
[32] C. H. Barnett and A. F. Cobbold, "Effects of age upon the mobility of human finger joints," *Ann. Rheum. Dis.*, vol. 27, pp. 175–177, 1968.
[33] R. L. Weber, K. V. Manning, and M. W. White, *College Physics*, 4th ed. New York: McGraw-Hill, 1965, p. 66.
[34] D. G. Kamper, E. G. Cruz, and M. P. Siegel, "Stereotypical fingertip trajectories during grasp," *J. Neurophysiol.*, vol. 90, pp. 3702–3710, 2003.
[35] J. M. Moran, J. H. Hemann, and A. S. Greenwald, "Finger joint contact areas and pressures," *J. Orthopaed. Res.*, vol. 3, pp. 49–55, 1985.
[36] L. Zollo, S. Roccella, E. Guglielmelli, M. C. Carrozza, and P. Dario, "Biomechatronic design and control of an anthropomorphic artificial hand for prosthetic and robotic applications," *IEEE/ASME Trans. Mechatronics*, vol. 12, no. 4, pp. 418–429, Aug. 2007.
[37] A. Chiri, F. Giovacchini, S. Roccella, N. Vitiello, E. Cattin, F. Vecchi, and M. C. Carrozza, "Handexos: Towards a support device for hand activities and telepresence," presented at the 10th ESA Workshop Advanced Space Technology Robotics Automation, ESTEC, Noordwijk, The Netherlands, 2008.

Azzurra Chiri received the M.S. degree in biomedical engineering (*cum laude*) from the University of Pisa, Pisa, Italy, in October 2007. Since November 2007, she has been with The BioRobotics Institute of the Scuola Superiore Sant'Anna, Pisa, where she is currently working toward the Ph.D. degree in biorobotics.

Her current research interests include biomedical robotics, rehabilitation engineering, and wearable systems.

Nicola Vitiello (S'11) received the M.Sc. in biomedical engineering (*cum laude*) from the University of Pisa, Pisa, Italy, in July 2006, and the Ph.D. degree in biorobotics from the Scuola Superiore Sant'Anna, Pisa, in December 2010.

He is involved in research at The BioRobotics Institute of the Scuola Superiore Sant'Anna. In 2006, he participated in the IX European Space Agency (ESA) Student Parabolic Flight Campaign as a Team Member. In 2008, he participated in the first ESA Lunar Robotics Challenge as the Ph.D. Student Member. His current research interests include the development of control algorithms for wearable robotic devices for human motion assistance and rehabilitation.

Francesco Giovacchini received the M.S. degree in mechanical engineering from the University of Pisa, Pisa, Italy, in 2006.

Since January 2007, he has been with The BioRobotics Institute of the Scuola Superiore Sant'Anna, Pisa, Italy. His research interests include the field of biomechatronics, and, more specifically, the development of robotic platforms and wearable devices for rehabilitation and neurobotics.

Stefano Roccella received the Laurea degree in aeronautical engineering from the University of Pisa, Pisa, Italy, and the Ph.D. degree in robotics from the University of Genova, Genoa, Italy, in March 2006.

In 1999, he joined The BioRobotics Institute of the Scuola Superiore Sant'Anna, Pisa, Italy, as a Research Assistant, where he is currently the Ph.D. Technical Research Manager. His research interests include the fields of mechatronic systems, humanoid robotics, biomedical robotics, rehabilitation engineering, biomechatronics, and MEMS design and development.

Fabrizio Vecchi (M'04) received the University degree (*Laurea*) in electrical engineering from the University of Pisa, Italy, in 1999, and the Ph.D. degree in Robotics from the University of Genova, Genoa, Italy, in 2003.

He is currently a Postdoctoral Research Scientist at The BioRobotics Institute of the Scuola Superiore Sant'Anna, Pisa, Italy. During his career, he has participated in the design and development of human–machine interfaces, biomechatronic prosthetic and robotic hands, passive and active orthoses, flexible sensory skin, and technical assistive devices. He is a Coinventor of seven national and international patents, and is a coauthor of more than 40 scientific papers published in ISI journals and in proceedings of international conferences.

Maria Chiara Carrozza (M'04–A'06) received the M.Sc. degree in physics from the University of Pisa, Pisa, Italy, in 1990, and the Ph.D. degree in bioengineering from the Scuola Superiore Sant'Anna (SSSA), Pisa, in 1994.

She is currently a Full Professor of Biomedical Engineering and Robotics at the SSSA. Since November 2007, she has also been the Director of SSSA. She was a Visiting Professor at the Technical University of Vienna, Vienna, Austria, teaching a graduate course entitled Biomechatronics, and she was involved in the scientific management of the Italy–Japan joint laboratory for Humanoid Robotics ROBOCASA, Waseda University, Tokyo, Japan. Her research interests include ambient assisted living, biorobotics, rehabilitation engineering, bionics, cybernetic hands, humanoid robotics, systems for functional replacements and augmentation, biomechatronic interfaces, tactile sensors, and artificial skin. She is the author of numerous scientific papers (more than 60 ISI papers and more than 100 papers in refereed conference proceedings) and of 12 national and international patents.